ELSEVIER

Materials Science and Engineering A318 (2001) 144–154

MATERIALS SCIENCE & ENGINEERING A

www.elsevier.com/locate/msea

Precipitation of Al_3Sc in binary Al–Sc alloys

Gabriel M. Novotny [1], Alan J. Ardell *

Department of Materials Science and Engineering, School of Engineering and Applied Science, University of California, 405 Hilgard Avenue, 6531 Boelter Hall, Los Angeles, CA 90095, USA

Received 21 September 2000; received in revised form 5 March 2001

Abstract

The precipitation of coherent Al_3Sc particles in Al–Sc alloys containing 0.06, 0.12 and 0.18 at.% Sc was investigated. The alloys were aged at 350°C for times up to 4663 h and the kinetics of particle growth, the particle size distributions and the evolution of particle morphology were measured and evaluated using transmission electron microscopy. Al_3Sc precipitates did not nucleate homogeneously in the most dilute alloy; this result was unexpected because 0.06 at.% Sc exceeds the solubility limit at 350°C. Persistent dislocation networks were observed in the alloy containing 0.12 at.% Sc under normal solution treatment conditions (e.g. 1 h at 600°C) and the dislocations acted as heterogeneous nucleation sites. The dislocations were ultimately eliminated using a very long solution treatment time of ~ 70 h near the melting temperature. Aging of both of the more concentrated alloys produced coherent precipitates. At short aging times the particles in the alloy containing 0.12% Sc were cauliflower-shaped and became spherical at longer times. At 4663 h some of the precipitates in this alloy were cuboidal, while others appear to have become semicoherent. The precipitates in this alloy were highly resistant to coarsening, and their size distributions were for the most part narrower than that predicted by the classical theory of Lifshitz, Slezov and Wagner (the LSW theory). The shapes of the precipitates in the alloy containing 0.18% Sc evolved from spherical to cuboidal with increasing aging time. The kinetics of growth of the precipitates in this alloy were consistent with the predictions of the LSW theory, the average size, $\langle r \rangle$, increasing with aging time, t, according to an equation of the type $\langle r \rangle^3 \simeq kt$. The experimentally measured rate constant, k, was in very good agreement with that calculated theoretically for this alloy.

Keywords: Al–Sc; Precipitation; Coarsening; Microstructire; Kinetics

1. Introduction

Considerable experimental work has been done to test the predictions of the theory of diffusion-controlled Ostwald ripening, first published by Lifshitz and Slezov [1] and Wagner [2] about 40 years ago. Strictly speaking, the so-called LSW theory is not applicable in a real system because one of its major implicit premises is that the equilibrium volume fraction, f_e, of the dispersed phase is infinitesimally small. In a real alloy containing a finite volume fraction of precipitates the diffusion fields of the particles will interact and affect the kinetics of coarsening. The predicted effect of f_e is always to increase the rate of coarsening, which is manifested through an increase in the rate constant, k, in the well-known asymptotic rate law $\langle r \rangle \approx (kt)^{1/3}$, where $\langle r \rangle$ is the average radius of the particles at time t [1,2]. Lifshitz and Slezov themselves recognized that their theory should be modified in some way to account for the finite volume fraction of the dispersed phase, and discussions of many of the proposed modifications of the LSW theory can be found in review articles by Ardell [3] and Voorhees [4,5]. In all cases k increases as f_e increases, but the dependence of k on f_e differs from one theory to another. The distribution of particle sizes (PSD) also becomes increasingly broad as f_e increases, and the predicted shape of the distribution also depends on the theory.

Most investigations of coarsening behavior in alloys begin with precipitation from a supersaturated solid solution, coarsening being the final stage of the precipi-

* Corresponding author. Tel.: +1-310-8257011; fax: 1-310-2067353.

E-mail address: aardell@ucla.edu (A.J. Ardell).

[1] Present address: Vitesse Semiconductor Corporation, 741 Calle Plano, Camarillo, CA 93012, USA.

0921-5093/01/$ - see front matter
PII: S0921-5093(01)01326-0

tation process. In alloy systems of this type none of the theories published to date is capable of predicting the dependence of k on f_e or the PSDs observed experimentally. One source of the disagreement may be the role of coherency strains induced by the lattice mismatch between the matrix and precipitate phases. These strains produce elastic self-energy, which influences the shapes of the particles, and can also induce elastic interactions among them, producing strong spatial correlations that usually involve alignment of the precipitates along elastically soft crystallographic directions. The magnitudes of these self and interaction energies are proportional to the square of the lattice misfit, ε, where $\varepsilon = (a_p - a_m)/a_m$, a_p and a_m being the lattice parameters of the precipitate and matrix phases, respectively.

The influence of elastic energy on precipitate morphology and spatial distributions is evident in studies of coarsening of γ'-type precipitates in Ni-base alloys. The γ' phase has the Cu_3Au ($L1_2$) crystal structure and is exemplified by Ni_3Al, the coarsening behavior of which has been investigated more thoroughly than any other dispersed phase. Similar γ'-type phases exist in the binary Ni–Ga, Ni–Ge, Ni–Si and Ni–Ti systems (the $L1_2$ form of Ni_3Ti is metastable). There appears to be a reasonable, though imperfect [6], correlation between the magnitude of ε and the shapes of the γ' precipitates. For small values of ε the particles remain spherical to larger sizes and tend to interact less strongly. At larger values of ε the particles evolve from spheres to cubes at increasingly smaller sizes. The intermediate shape between the sphere and the cube is called the cuboidal shape, which refers to a cube with rounded corners and edges, the flat portions of the interfaces being parallel to $\langle 100 \rangle$. At larger values of ε the elastic interactions become stronger, causing alignment along $\langle 100 \rangle$ and eventual coalescence. The effects of volume fraction and coherency strain are synergistic in the sense that the elastic interactions become increasingly pronounced as f_e increases. For this reason yet another shape transition, from a cube with nearly flat interfaces to one with concave interfaces (the concave cuboidal shape), is really evident only in alloys in which f_e is small, < 0.04 as a rule of thumb.

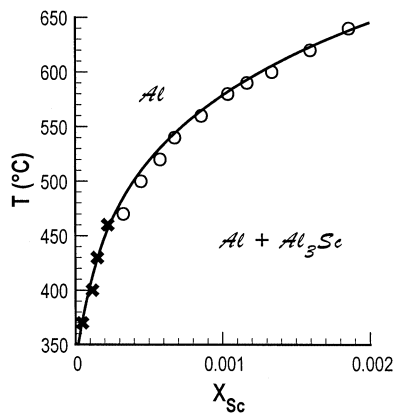

Fig. 1. The Al-rich region of the Al–Sc phase diagram. The data are from: ○ Fujikawa et al. [9]; × Jo and Fujikawa [10].

Owing to the generally large solubility of Al, Ga, Ge, Si and Ti in Ni (in excess of 8 at.% at practical aging temperatures), and to the difficulty of preparing extremely homogeneous alloys by conventional ingot-metallurgy processing, it is not easy to prepare alloys with small volume fractions of γ' precipitates. Homogeneity is especially important if systematic control of f_e is an experimental objective, especially when f_e is small. Since the LSW theory is valid only at vanishingly small values of f_e, it would be highly advantageous to investigate coarsening in an alloy in which $f_e << 0.04$. In such alloys we might also entertain the hope that the precipitates will be so far apart that they cannot interact elastically. Al–Sc alloys are potentially suitable for such investigations and have received attention recently due to the improved mechanical properties attributed to the precipitation of Al_3Sc particles in the Al matrix [7,8].

There are several reasons for the suitability of Al–Sc alloys for investigating coarsening at very small values of f_e: (1) the particles in equilibrium with the α-Al solid solution have the stoichiometric composition Al_3Sc, which has the $L1_2$ crystal structure and is therefore easy to image by dark-field transmission electron microscopy (TEM) using a superlattice reflection; (2) the solubility of Sc in Al is very small, as is evident from the Al-rich region of the Al–Sc phase diagram shown in Fig. 1, and the solvus curve is known quite accurately [9,10]. The maximum solubility of Sc in Al is 0.21 at.% at 655°C, and a simple calculation using the lever rule shows that the maximum possible value of f_e lies between 0.008 and 0.009; (3) the lattice mismatch is quite large ($\varepsilon = 0.01365$ calculated using the reported [7] value of $a_p = 0.4105$ nm), hence the coherency strains could influence the particle morphology as they do in Ni-base alloys. However, since f_e is nearly two orders of magnitude smaller than in Ni-base alloys the elastic interactions should be small; (4) though Al–Sc alloys might be considered as rather exotic, they have been surprisingly well characterized. In addition to the parameters of the alloy system already noted, the diffusivity of Sc in Al has been measured [11], the elastic constants of polycrystalline Al_3Sc are known [12,13] and the single-crystal elastic constants have been calculated theoretically [14].

In principle, investigations of the coarsening of Al_3Sc precipitates also present an excellent opportunity to determine whether the rate constant for coarsening varies as $f_e^{1/2}$ or $f_e^{1/3}$ as f_e approaches zero. Different theories predict these two kinds of behavior in the limit of zero volume fraction [3–5] (see also a recent paper by Mandayam et al. [15] for a discussion of this issue),

Table 1
Concentrations of Sc and volume fractions of Al_3Sc in the alloys investigated

wt. frac. Sc	at. frac. Sc	f_e (at 350°C)
0.0010	0.0006	0.0019
0.0020	0.0012	0.0044
0.0030	0.0018	0.0069

but the experimental data needed to test these different hypotheses have never been generated. One of the original intentions of this research project was to explore the dependence of k on f_e in the regime of very small f_e. There was some expectation of eventual success based on the work of Hyland [16], who investigated nucleation in alloys similar in concentration to those used in this work. However, we found that coarsening behavior of the kind we expected was seen in only one of the three alloys. In this paper we report our observations of the precipitation of Al_3Sc in all the alloys and point out that its behavior is unexpected in several respects.

2. Experimental procedures

Three aluminum-scandium alloys, containing 0.06, 0.12 and 0.18 at.% Sc (0.1, 0.2, and 0.3 wt.% Sc), were provided by Dr R.W. Hyland of the ALCOA Technical Center. We will refer to these as Alloy 1, Alloy 2 and Alloy 3, respectively. The alloys were obtained in the form of rolled sheets, with thicknesses ranging from 0.5 to 1.0 mm. We further cold-rolled the sheets to thicknesses ranging from 250 to 350 μm. Specimens were then homogenized at temperatures in the range 635–650°C for over 1 h to produce a solid solution, and quenched into water.

All the alloys were aged at 350°C. It is evident from Fig. 1 that all three solution-treated alloys are supersaturated at this aging temperature, at which f_e is calculated to vary from ~ 0.002 to ~ 0.007 (Table 1). The solution-treated specimens were aged in air inside a horizontal clamshell furnace. To minimize the temperature gradient, four thick rings of Al were placed inside the furnace to provide thermal ballast and positioned to minimize the temperature gradient. This resulted in a temperature gradient of less than 1°C over a distance of 20 mm, and a temperature fluctuation of no greater than ± 0.5°C. The specimens were contained inside a stoppered pyrex glass tube during aging to eliminate convection, and after the desired aging time was reached they were withdrawn and generally air-cooled. The slow kinetics of precipitation in Al–Sc alloys made water-quenching of the aged specimens unnecessary.

Hyland [16] found that nucleation in an alloy containing 0.11 at.% Sc aged at 343°C essentially ended after ~ 1000 s. We therefore expected similar behavior, at least in Alloys 2 and 3, so the first aging time chosen was 24 h. This was followed by further aging times separated by 24 h intervals. Preliminary investigations indicated that Al_3Sc precipitates did not nucleate homogeneously in Alloy 1 even after aging times of 624 h. Instead, Al_3Sc nucleated only heterogeneously on grain boundaries. Spatially uniform distributions of coherent precipitates were observed in both Alloy 2 and Alloy 3. However, nearly all the precipitates in Alloy 2 were found to be growing on dislocations, as shown in Fig. 2a. It was therefore necessary to eliminate the large dislocation density in Alloy 2 to avoid heterogeneous nucleation of Al_3Sc on dislocations, and this turned out to be somewhat problematic because the dislocation

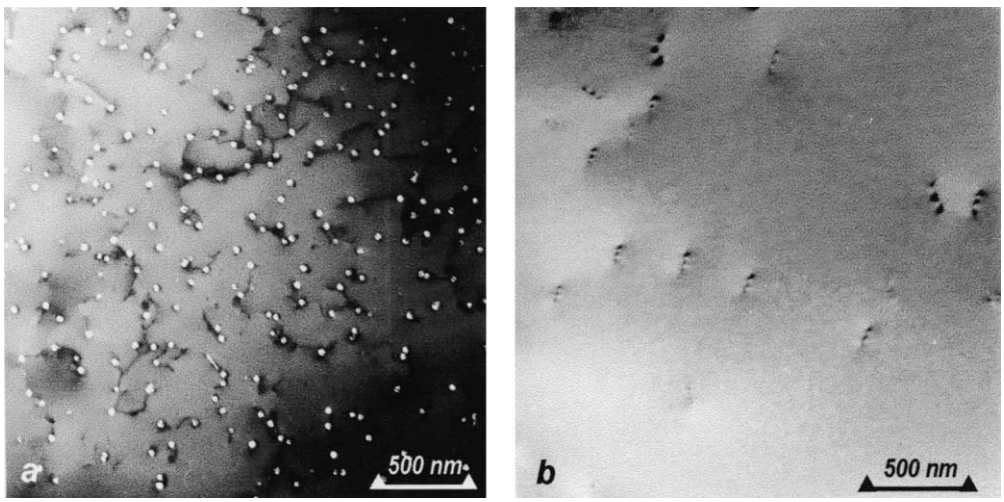

Fig. 2. a) Nucleation on dislocations in Alloy 2 aged for 144 h at 350°C. In this dark-field image taken using a superlattice reflection the dislocations appear as slightly dark lines with respect to background. (b) Dislocation-free microstructure in Alloy 2 solution treated for 70.5 h at 651°C and air cooled.

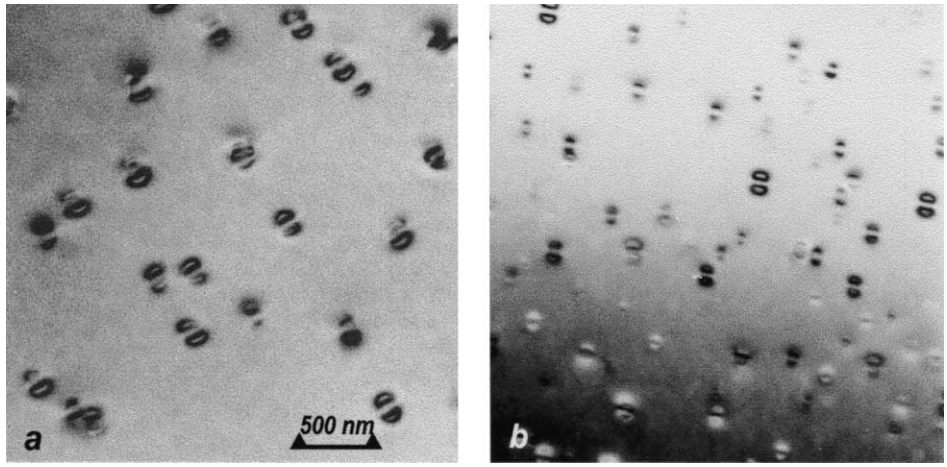

Fig. 3. Bright field TEM micrographs of coherency strains at coherent Al_3Sc precipitates. (a) Alloy 2 aged for 168 h and (b) Alloy 3 aged for 552 h.

density was surprisingly stable. Ultimately, the dislocation density was substantially reduced using a very long solution treatment time of 70.5 h at 651°C. This produced the nearly dislocation-free microstructure shown in Fig. 2b. In contrast to Alloys 1 and 2, homogeneous nucleation of Al_3Sc in Alloy 3 occurred readily, and no special solution treatment was needed to investigate the kinetics of precipitation in this alloy.

Following aging, disks 3 mm in diameter were punched from the sheets and abraded to thicknesses of 150–200 μm using # 600 emery paper. The disks were then dimpled electrochemically at 50 V DC to a thickness of ~15 μm using a solution of 45% H_2O, 20% HNO_3, 20% H_3PO_4, and 15% $HC_2H_3O_2$. Electron-transparent thin foils were produced by electrochemical polishing the dimpled disks at ~20 V d.c. in a solution of 30% HNO_3 in CH_3OH, cooled to −65°C by liquid nitrogen. After final perforation of the disks they were immediately rinsed in methanol and stored in a vacuum dessicator. TEM was performed using a JEOL 100 CX TEMSCAN microscope at an operating voltage of 100 keV. Dark-field images of the Al_3Sc precipitates were taken using a {100} superlattice reflection in a low index zone axis, typically [001].

The TEM negatives were digitized using a Mikrotek model ScanMaker 35t slide scanner and scanned at a resolution of 1820 dpi. The sizes of the precipitates were measured using the software package Image-Pro Plus for Windows, v. 1.0 and v. 3.0. The 'radius', r, of each particle was measured using the method described by Cho and Ardell [17], in which r is obtained from the formula $r = r_m(B+1)/2$. Here r_m is the radius of the largest circle that can be inscribed within the image of the particle and $B = a_1/a_2$, where a_1 and a_2 define the edges of the smallest rectangle that completely contains the particle within its boundary (a_1 is the longer of the two edges). This appears to be an unnecessarily circuitous process, but the software application provides direct measurements of r_m and B, not a_1 and a_2.

3. Results

The precipitates in both Alloys 2 and 3 exhibited the classic lobed strain-field diffraction contrast in bright field TEM images [18], as is evident in Fig. 3. The strain field contrast persisted up to 4663 h, which was the longest aging time used in our work. Fig. 4 shows the evolution with time of the Al_3Sc particles in Alloy 2. As is evident on viewing the images, there is no systematic increase of the particle size with aging time, as would be expected during all stages of precipitation. Instead, the particle size appears to fluctuate about some mean value. Hyland [16] reported that after 30 min of aging the nucleation stage was completed, albeit at a slightly lower temperature (343 cf. 350°C). This is approximately what is observed in Fig. 4, at least qualitatively, where the number of precipitates per unit volume appears to be essentially constant from 5 h of aging onward. The spatial distributions of the Al_3Sc particles appeared to be uniform at all aging times.

The evolution of the morphology of the precipitates in Alloy 2 is shown in Fig. 5 and Fig. 6. At early aging times (up to ~25 h) the particles were found to have a cauliflower-like shape. This unexpected shape was seen as early as 1 h, prior to the end of nucleation. After 25 h, however, the particles evolved into a more spherical shape; 'spheroidization' was complete at 72 h. At the longest aging time (4663 h) some evidence for partial loss of coherency was seen in the form of dark lines of contrast in the images of many of the precipitates. Examples are shown in Fig. 6, with the 'semicoherent' particles indicated by the solid arrows. We interpret these images as contrast due to an interface dislocation,

but it was not possible to verify this because these precipitates still exhibited quite strong coherency strain-field contrast. Precipitates with cuboidal shapes and flat interfaces parallel to $\langle 100 \rangle$ were also evident in the microstructure; examples are indicated by the dashed arrows in Fig. 6. The cuboidal particles were generally larger than the average size, while the 'semicoherent' precipitates tended to be about the average size.

Fig. 7 shows the evolution with aging time of the particle sizes, shapes and spatial correlations in Alloy 3. There is no doubt that the sizes of the particles increase with aging time in this alloy. Moreover, the shapes are definitely spherical when the particles are small, as is evident in Fig. 8, and appear to become cuboidal in shape as they grow to larger sizes, as in Alloy 2. Evidence for the cuboidal shape was seen at 1251 h, and is quite convincing after 3093 h (Fig. 8). There did not appear to be any significant tendency towards alignment along the cube directions in this alloy.

The data on both alloys are plotted as $\ln\langle r \rangle$ versus $\ln(t)$ in Fig. 9. A line with the slope of 1/3, representing the LSW theoretical prediction, is superimposed on the data. The data on Alloy 2 deviate considerably from theory, the particle sizes remaining essentially constant even to the longest aging time of just over 4600 h. In Alloy 3 the kinetics of growth of the Al_3Sc precipitates are much more consistent with the behavior predicted by the LSW theory. The plot of $\ln\langle r \rangle$ versus $\ln(t)$ for

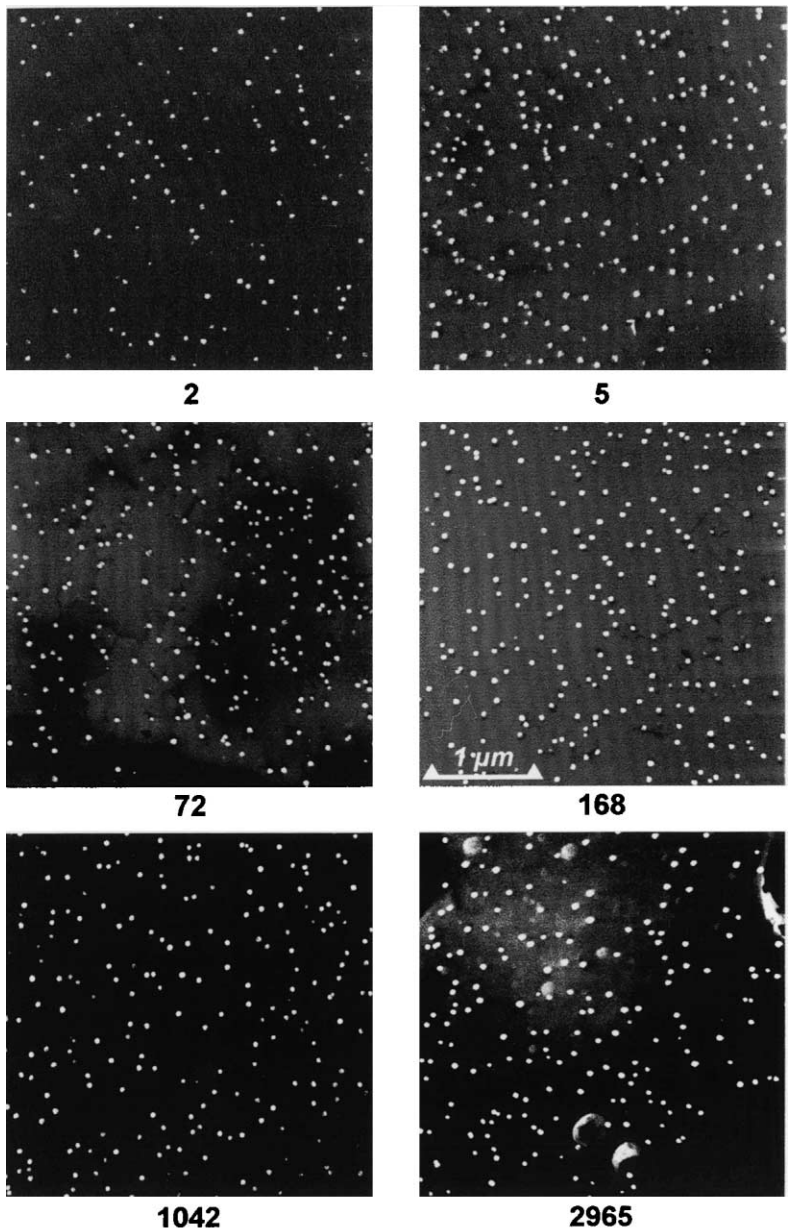

Fig. 4. Evolution of the Al_3Sc precipitate microstructure in Alloy 2. The number under each figure is the aging time in hours.

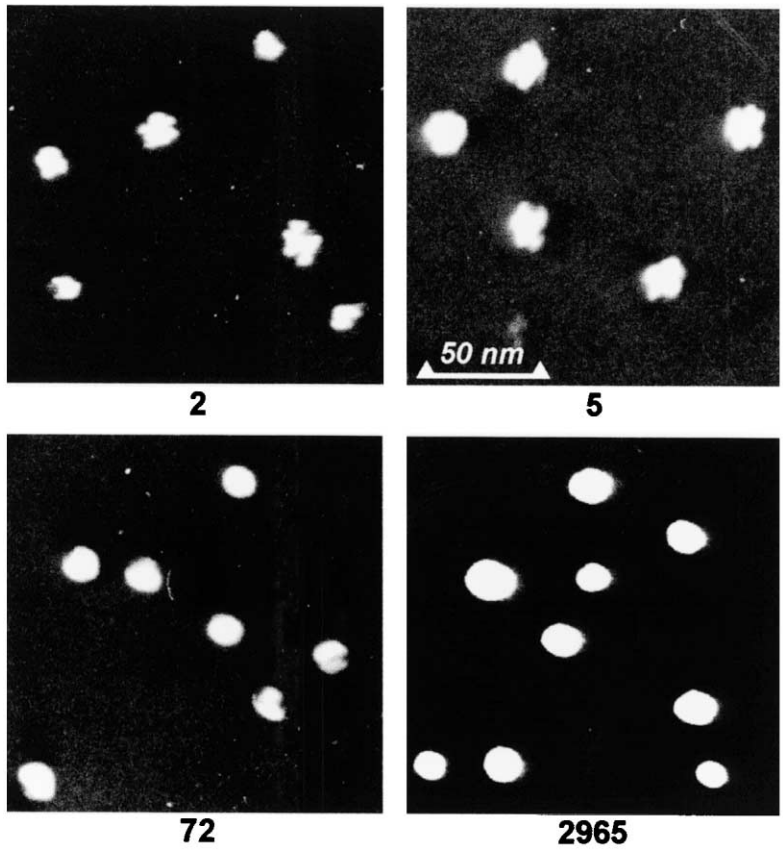

Fig. 5. Evolution of the shapes of the Al_3Sc particles in Alloy 2. The number under each figure is the aging time in hours.

Alloy 3 deviates slightly at early times, but approaches a slope of 1/3 as t increases. The data on Alloy 3 are re-plotted as $\langle r \rangle^3$ versus t in Fig. 10, where it is seen that approximately linear behavior is observed to the longest aging time (3096 h).

The particle size distributions (PSD) for Alloys 2 and 3 are shown in Fig. 11 and Fig. 12, respectively. The LSW prediction is superimposed upon each histogram. At early times, the PSDs in both alloys are in remarkably good agreement with the LSW distribution, but this agreement does not persist as a function of aging time. In Alloy 2 the distributions actually become narrower at aging times from 72 to 1042 h. The PSDs in Alloy 3, however, generally become broader with aging time. These trends are more evident on comparing the standard deviations of the PSDs, Σ, with that of the LSW theory ($\Sigma = 0.215$). These are shown in Fig. 13 for the 2 alloys where it is seen that the majority of values of Σ for Alloy 2 are smaller than 0.215, whereas those for Alloy 3 are greater than 0.215.

4. Discussion

Based on the results of Hyland [16], we expected that Al_3Sc precipitates in all three alloys would undergo the expected classical stages of homogeneous nucleation, growth and coarsening. This was clearly not the case, however, and we have no explanation for why the nucleation behavior of Al_3Sc in Alloy 2 was so different from what Hyland observed. An attempt was made to check the compositions of the alloys using energy dis-

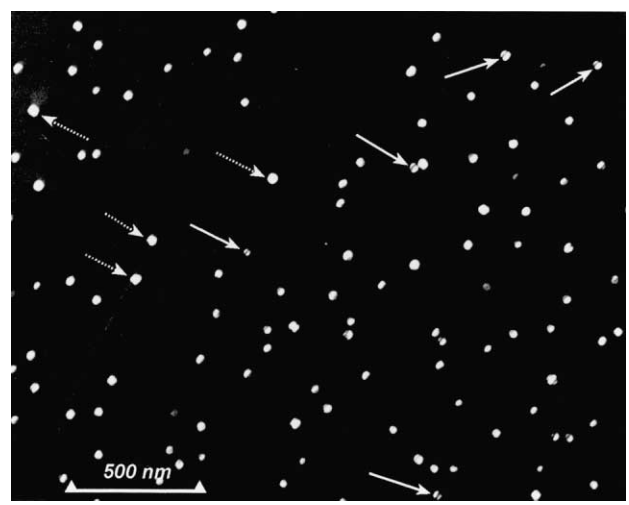

Fig. 6. Dark-field TEM image of the precipitate microstructure in Alloy 2 aged for 4663 h. The contrast at the particles indicated by the solid arrows is characterized by a dark line or arc running through it. The particles indicated by the dashed arrows are cuboidal in shape.

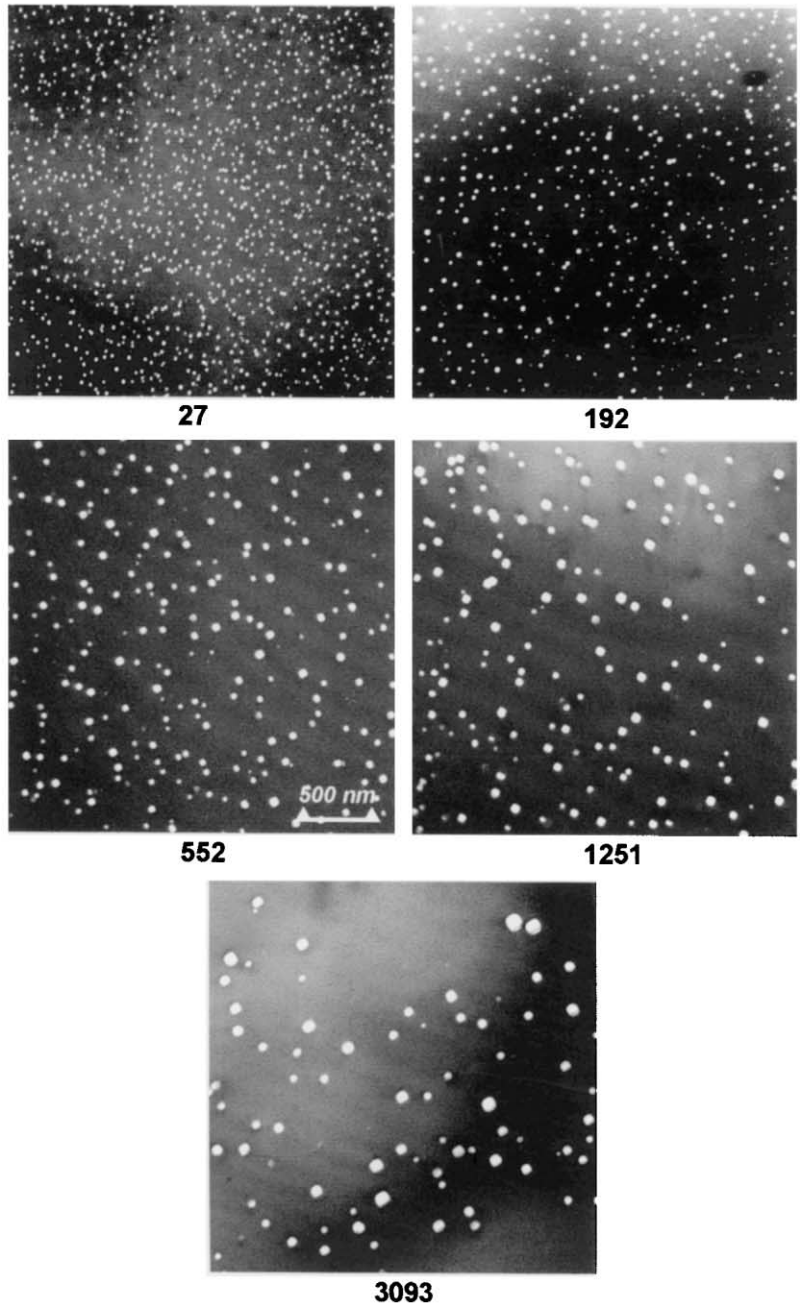

Fig. 7. Evolution of the Al_3Sc precipitate microstructure in Alloy 3. The number under each figure is the aging time in hours.

persive *X*-ray spectroscopy (EDS) to see if this could account for the very different behavior found by us and Hyland. EDS was performed using a Cambridge Stereoscan 250 scanning electron microscope operating at 20 keV equipped with a Kevex energy dispersive *X*-ray spectrometer and a beryllium ('SuperBeryllium™') window. The results indicated that the concentration of Sc definitely increased from Alloy 1 to Alloy 3, but quantitative analysis was not possible because of the small absolute values of the concentration of Sc in the three alloys.

The cauliflower shapes observed when the precipitates are very small (see Fig. 5) have not been reported in previously published work on Al–Sc alloys. The theoretical work of Lee [19] predicts the existence of cauliflower-shaped particles which are elastically softer than the matrix. These evolve from particles that are initially spherical (or, more appropriately circular, since Lee's calculations are 2-dimensional), which is exactly the opposite behavior to what we observe. Also, Al_3Sc precipitates are much harder elastically compared to the Al matrix in which they reside, as is evident from the

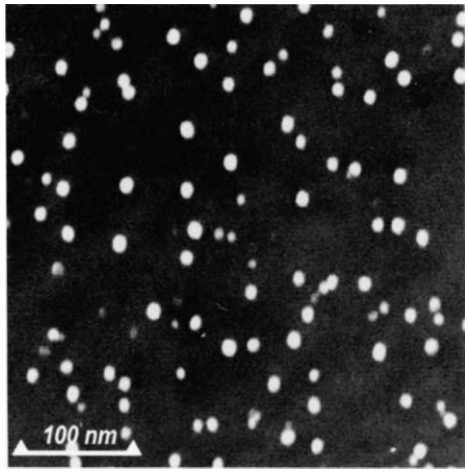

Fig. 8. Dark-field TEM micrograph illustrating the spherical shapes of small Al_3Sc particles in Alloy 3 aged for 27 h.

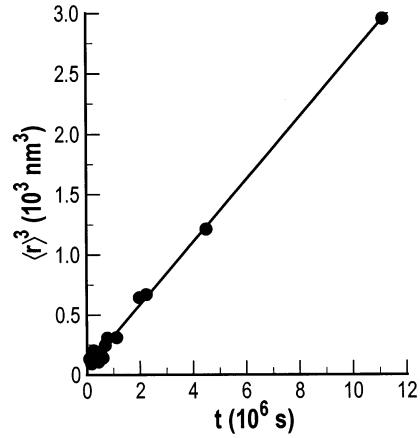

Fig. 10. The data on Alloy 3 in Fig. 9 plotted as $\langle r \rangle^3$ versus t.

data on the elastic constants, which are summarized in Table 2.

The cauliflower-shaped particles in Alloy 2 are evidently favored during nucleation, and suggest that nucleation might be heterogeneous, followed by a brief stage of dendritic growth. This suggestion is highly speculative because the nucleation sites are nowhere in evidence. The observation is nevertheless interesting because the initial shape of the precipitates is clearly metastable with respect to the equiaxed shape into which it evolves. The 2-dimensional theoretical calculations of Jou et al. [21] show that an elastically soft particle, initially dendritic in shape as a result of growth under a positive flux of solute, evolves to an equiaxed shape when the flux of solute is removed. Except for the relative magnitudes of the elastic constants of the precipitate and matrix phases in Al–Sc alloys, this predicted behavior is very similar to what we observe.

It appears that the particles in Alloy 2 do not coarsen at all, and there is no reasonable explanation for the remarkable stability of the dispersion of Al_3Sc precipitates in this alloy. Such behavior is not noted in earlier work, even in alloys more dilute than Alloy 2. Berezina et al. [22], reported that their data on the kinetics of growth of Al_3Sc precipitates in an alloy comparable in composition to Alloy 3 obey a kinetic law of the type $\langle r \rangle^2 \propto t$. However, theirs is the only other work to report any deviations from diffusion-controlled coarsening behavior in Al–Sc alloys.

Having noted the unexpected stability of the Al_3Sc precipitate dispersion in Alloy 2, it is interesting to compare the experimentally measured rate constant, k, obtained from the slope of the linear fit to the data in Fig. 9 with the value expected theoretically from the equation [23,24]

$$k = \frac{8X_{\alpha e}(1 - X_{\alpha e})\sigma D V_{m\beta}}{9RT(X_{\beta e} - X_{\alpha e})^2} \quad (1)$$

where $X_{\alpha e}$ and $X_{\beta e}$ are the equilibrium concentrations of Sc in the matrix and Al_3Sc phases, respectively, σ is the interfacial free energy, D is the coefficient of solute diffusion in the matrix, $V_{m\beta}$ is the partial molar volume of Sc in Al_3Sc and the product RT has its usual

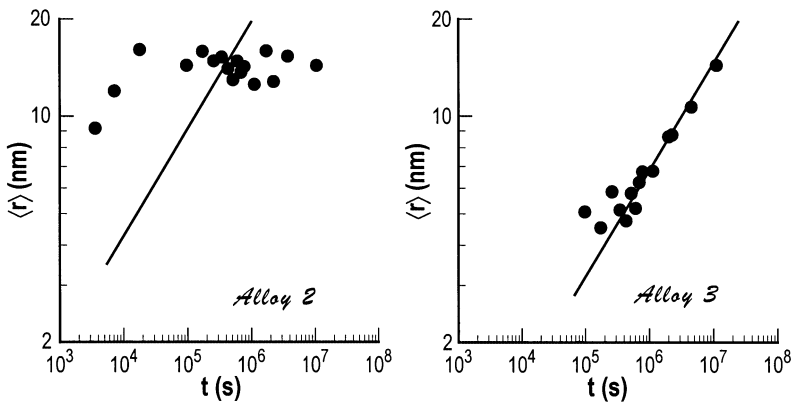

Fig. 9. Log-log plots of the average particle radius, $\langle r \rangle$, versus aging time for Alloy 2 and Alloy 3. A line with slope = 1/3 is superimposed on each figure.

meaning. In Eq. (1) the matrix phase is assumed to be an ideal solid solution. Since the hard-sphere radius of Sc is significantly larger than that of Al, $V_{m\beta}$ was estimated with the assumption that the ratio of the radii of the two atoms is the same in Al_3Sc as it is for the pure elements, namely 1.1516. The molar volume of Al_3Sc is $N_A a_p^3 = 4.166 \times 10^{-5}\ m^3\ mol^{-1}$, where N_A is Avogadro's number and $a_p = 0.4105$ nm. The partial molar volumes of Sc and Al are therefore $1.4054 \times 10^{-5}\ m^3\ mol^{-1}$ and $9.2025 \times 10^{-6}\ m^3\ mol^{-1}$, respectively. From the data of Jo and Fujikawa [10], we obtain $X_{\alpha e} = 3.884 \times 10^{-5}$ at 350°C. The tracer diffusion coefficient of Sc in Al has been measured recently by Fujikawa [11], who reported the result $D = 5.31 \times 10^{-4} \exp(-173\,000/RT)\ m^2\ s^{-1}$, with the activation energy in J mol^{-1}. At 623 K we obtain $D = 1.658 \times 10^{-18}\ m^2\ s^{-1}$. The precise magnitude of σ is not known, but values obtained from the analysis of experimental data include those of Hyland [16] (94 ± 23 mJ m^{-2}) and Jo and Fujikawa [10] (41–63 mJ m^{-2}). Asta et al. [25] have calculated the Al/Al_3Sc interfacial energies for {100} and {111} interfaces, producing values of 192 and 226 mJ m^{-2}, respectively. These are valid at 0 K, but the calculated temperature dependence of σ is weak to 650 K [25].

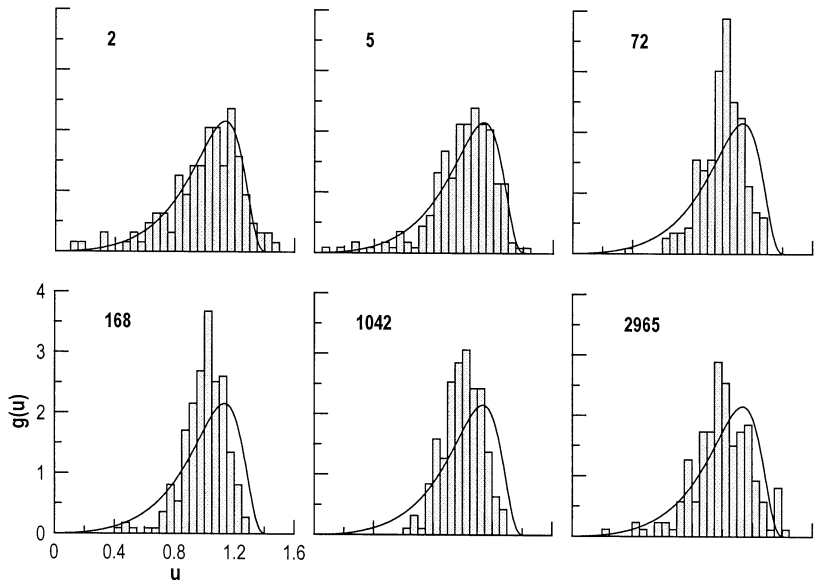

Fig. 11. Histograms of the particle size distributions as a function of aging time in Alloy 2. The number in each figure is the aging time in hours, and the LSW distribution is superimposed on each figure.

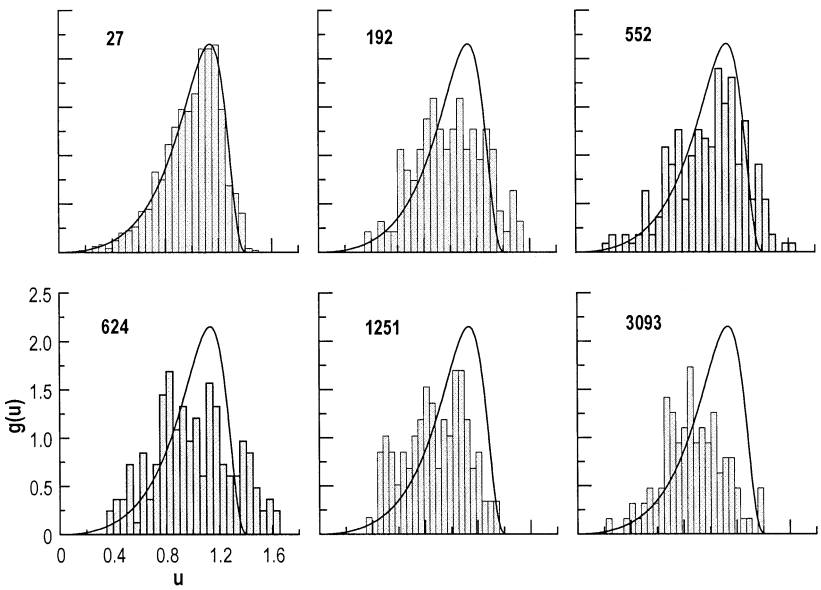

Fig. 12. Histograms of the particle size distributions as a function of aging time in Alloy 3. The number in each figure is the aging time in hours, and the LSW distribution is superimposed on each figure.

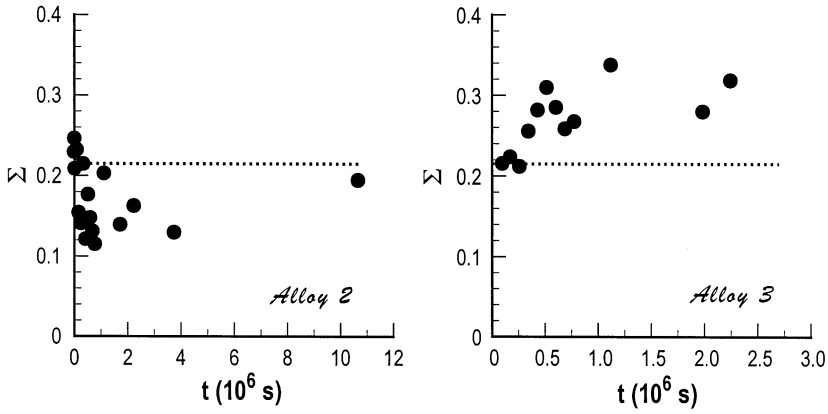

Fig. 13. The standard deviation, Σ, of the particle size distribution versus aging time, t, for Alloy 2 and Alloy 3.

Assuming that σ lies in the range $0.06 < \sigma < 0.21$ J m^{-2} and taking $X_{\beta e} = 0.25$, the upper and lower limits to the value of k at 623 K should be between 1.49×10^{-31} and 5.22×10^{-31} m^3 s^{-1}. From the slope of the curve in Fig. 10 we find $k = 2.6 \times 10^{-31}$ m^3 s^{-1}, which lies comfortably between the two calculated limits. An alternative way of looking at this is that the experimentally measured value of k yields the value $\sigma = 0.105$ J m^{-2}, which compares quite favorably with all the previously reported values.

As a result of this calculation it is reasonable to ponder whether the resistance to coarsening of the precipitate dispersion in Alloy 2 is more unusual than the unexpectedly rapid coarsening of the dispersion in Alloy 3. There is no solution to this conundrum based on the work done in this investigation. We can only conclude that the coarsening behavior of Al_3Sc precipitates is unexpectedly complex, and more work is needed to sort out the reasons for the unusual behavior.

5. Summary

The precipitation of Al_3Sc particles in Al–Sc alloys containing 0.06, 0.12 and 0.18 at.% Sc was investigated. The kinetics of precipitation and the morphologies of the precipitates were measured using TEM. The kinetics of particle growth were quantitatively consistent with diffusion-controlled coarsening kinetics only in Alloy 3. The shapes of the coherent Al_3Sc particles in this alloy evolved from spherical to cuboidal with increasing aging time. The particle size distributions were in excellent agreement with those of the LSW theory at early aging times. At longer aging times the distribution became broader, but this behavior is not unusual compared with other results in the literature.

Al_3Sc precipitates were highly resistant to coarsening in Alloy 2. At the earliest aging times, most probably still in the nucleation and/or growth stages of decomposition, the particles were cauliflower shaped. The shapes became approximately spherical as aging progressed, and the larger particles eventually became cuboidal in shape after the longest aging times used in this work (4663 h). Some evidence for partial loss of coherency was also found at the longest aging time. The kinetic behavior is difficult to reconcile with the current theories of nucleation, growth and coarsening, as well as with other data in the literature. The particle size distributions were also generally narrower than that predicted by the LSW theory; this behavior is also rather unusual. The tendency of the cauliflower-shaped Al_3Sc precipitates to become more equiaxed and nearly spherical in shape with increasing aging time is in semiquantitative agreement with the 2-dimensional numerical simulations of Jou et al. [21].

Acknowledgements

The authors are grateful to the National Science Foundation and Dr B.A. MacDonald for financial support of this research under grant # DMR-9526238. We thank Dr R.W. Hyland, Jr of Alcoa for providing the alloys used in this investigation and for helpful discussions on the results. We are very grateful to Professor D.N. Seidman of Northwestern University for pointing out an error in our original Eq. (1) and for bringing the recent data of Fujikawa [11] to our attention.

Table 2
Young's modulus, E, shear modulus, G, and bulk modulus, K, all in GPa, for pure Al and Al_3Sc

Phase	E	G	K	Ref
Al	70.3	26.1	76.5	[20]
Al_3Sc	166	68	99	[12]
Al_3Sc	164.2	68.4	91.5	[13]

References

[1] I.M. Lifshitz, V.V. Slezov, J. Phys. Chem. Solids 19 (1961) 35.
[2] C. Wagner, Z. Elektrochem. 65 (1961) 581.
[3] A.J. Ardell, in: G.W. Lorimer (Ed.), Phase Transformations'87, The Institute of Metals, London, 1988, p. 485.
[4] P.W. Voorhees, J. Stat. Phys 38 (1985) 231.
[5] P.W. Voorhees, Annu. Rev. Mater. Sci. 22 (1992) 197.
[6] A.J. Ardell, D.M. Kim, in: P.E.A. Turchi, A. Gonis (Eds.), Phase Transformations and Evolution in Materials, TMS, Warrendale, PA, 2000, pp. 309–320.
[7] N. Blake, M.A. Hopkins, J. Mat. Sci. 20 (1985) 2861.
[8] B.A. Parker, Z.F. Zhou, P. Nolle, J. Mat. Sci. 30 (1995) 452.
[9] S.-I. Fujikawa, M. Sugaya, H. Takei, K.-I. Hirano, J. Less-Common Met. 63 (1979) 87.
[10] H.-H. Jo, S.-I. Fujikawa, Mat. Sci. and Eng. A171 (1993) 151.
[11] S.-I. Fujikawa, Defect and Diffusion Forum 143-147 (1997) 115.
[12] E.P. George, J.A. Horton, W.D. Porter, J.H. Schneibel, J. Mater. Res. 5 (1990) 1639.
[13] R.W. Hyland Jr., R.C. Stiffler, Scripta Metall. Mater. 25 (1991) 473.
[14] C.L. Fu, J. Mater. Res. 5 (1990) 971.
[15] H. Mandyam, M.E. Glicksman, J. Helsing, S.P. Marsh, Phys. Rev. E 58 (1961) 2119.
[16] R.W. Hyland Jr., Met. Trans. A 23A (1992) 1947.
[17] J.-H. Cho, A.J. Ardell, Acta Mater. 45 (1997) 1393.
[18] M.F. Ashby, L.M. Brown, Philos. Mag. 8 (1963) 1083.
[19] J.K. Lee, Metall. Mater. Trans. A 27A (1996) 1449.
[20] M.A. Meyers, K.K. Chawla, Mechanical Behavior of Materials, Prentice-Hall, Upper Saddle River, NJ, 1999, p. 92.
[21] H.-J. Jou, P.H. Leo, J.S. Lowengrub, J. Computational Phys. 131 (1997) 109.
[22] A.L. Berezina, V.A. Volkov, B.P. Domashnikov, S.V. Ivanov, K.V. Cuistov, Metallofizika 12 (1990) 72.
[23] H.A. Calderon, P.W. Voorhees, J.L. Murray, G. Kostorz, Acta Metall. Mater. 42 (1994) 991.
[24] A.J. Ardell, Interface Sci. 3 (1995) 119.
[25] M. Asta, S.M. Foiles, A.A. Quong, Phys. Rev. B 57 (1998) 1.